New measurements of properties of the Ω^- hyperon

K. B. Luk,[a] A. Beretvas, L. Deck,[b] T. Devlin, R. Rameika,[c] and R. Whitman[d]
Department of Physics and Astronomy, Rutgers—The State University, P.O. Box 849, Piscataway, New Jersey 08854

R. Handler, B. Lundberg,[e] L. Pondrom, M. Sheaff, and C. Wilkinson[f]
Physics Department, University of Wisconsin, Madison, Wisconsin 53706

P. T. Cox,[g] E. C. Dukes,[h] J. Dworkin,[i] and O. E. Overseth
Department of Physics, University of Michigan, Ann Arbor, Michigan 48109

K. Heller
School of Physics and Astronomy, University of Minnesota, Minneapolis, Minnesota 55455
(Received 12 June 1987; revised manuscript received 12 February 1988)

We have obtained a sample of 1743 reconstructed $\Omega^- \to \Lambda K^-$ events produced by protons on a Be target at production angles of 5.0 and 7.5 mrad. The Ω^- lifetime, based on a subset of 1096 events, was measured to be $\tau(\Omega^-)=(0.811\pm0.037)\times10^{-10}$ sec, where the uncertainty is statistical and the systematic uncertainty is estimated to be small. The helicity of the daughter Λ yielded the product of asymmtery parameters $\alpha_\Lambda\alpha_\Omega=-0.022\pm0.051$ which, in turn, yields $\alpha_\Omega=-0.034\pm0.079$. The average daughter-$\Lambda$ polarization in the decay region was measured to be $P_\Lambda=0.12\pm0.08$ approximately perpendicular to the charged-hyperon beam line. The Ω^- polarization in the same region, i.e., after the precession magnet, depends on the sign of γ_Ω, which is unknown at present. The two possibilities are $P_\Omega=P_\Lambda$ if $\gamma_\Omega\approx+1$ and $P_\Omega=-\frac{5}{3}P_\Lambda$ if $\gamma_\Omega\approx-1$. The magnitude of the polarization vector is only 1.5 standard deviations different from zero, and this prevented a meaningful measurement of the Ω^- magnetic moment. If the broken-SU(6) prediction for the moment, $\mu(\Omega^-)=-1.83\mu_N$, is assumed to be true, then the precession of the Ω^- in the magnetic field is small and the values of P_Ω above are also true at the production target. If this polarization is different from zero and correct in sign, then it cannot be simultaneously reconciled with theoretical predictions for the sign of γ_Ω and for the sign of the production polarization. On the other hand, if the polarization is zero no inconsistency exists.

I. INTRODUCTION

We have collected a sample of 1743 Ω^- hyperons produced by 400-GeV protons in the reaction $p+\mathrm{Be}\to\Omega^-+X$. This paper describes an analysis of these data to study the production polarization and decay of the Ω^-.

The data were obtained in a series of charged-hyperon measurements[1–4] performed at Fermilab. The Ω^- events were collected in the same data runs with a large sample of Ξ^- events.[3,4] The experimental procedures and equipment were identical for the two samples. Section II will describe briefly these aspects of the measurement. The geometric and kinematic reconstruction for the two samples was quite similar, and Sec. III deals mainly with those aspects of the reconstruction unique to the Ω^-. The lifetime exhibited by this sample of Ω^-'s is consistent with the published results of other workers, and this is discussed in Sec. IV. The first measurement of the polarization of inclusively produced Ω^- is presented in Sec. V, along with an analysis of the helicity of the daughter Λ which confirms existing results for the asymmetry parameter in the decay.

The experimental setup was designed for measurements of the magnetic moments of other hyperons by the precession of their polarization vectors in a magnetic field. Thus, it had the potential of measuring the Ω^- magnetic moment. Since the Ω^- polarization vector differs from zero by only 1.5 standard deviations, no significant measurement of μ_Ω is claimed. In order to preclude any overinterpretation of the polarization data, a full discussion of this topic is presented in Sec. V.

II. EXPERIMENTAL APPARATUS AND PROCEDURES

Figure 1 shows plan and elevation views of the apparatus used to collect the data for this experiment. It has been described in other publications,[1–4] and in even more detail in Refs. 5–8. The experiment was performed in the *M*2 hyperon beam of the Meson Laboratory at Fermilab. The hyperon-beam channel and detection apparatus were arranged to collect samples of Ω^- and Ξ^- through the decay processes

$$\Omega^- \to \Lambda K^-, \quad \Lambda \to p\pi^- \tag{2.1}$$

and

$$\Xi^- \to \Lambda\pi^-, \quad \Lambda \to p\pi^- . \tag{2.2}$$

Because the proton is the most massive of the final-state particles, it usually carries most of the momentum of the

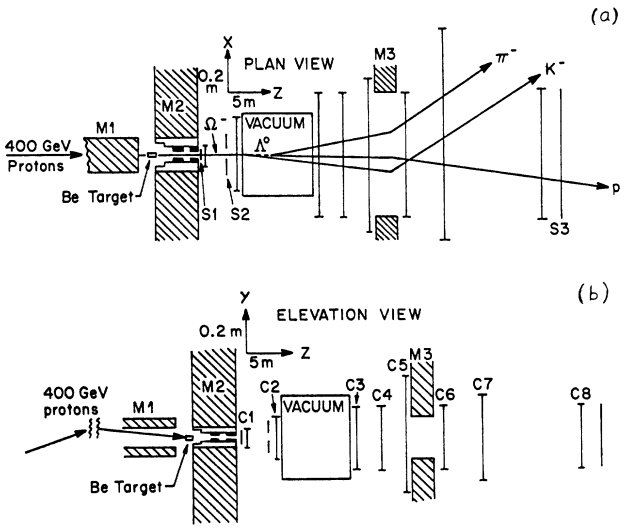

FIG. 1. (a) Plan and (b) elevation views of the spectrometer with a typical event topology shown. M_1–M_3 are dipole magnets, S_1–S_3 are scintillation counters, and C_1–C_8 are multiwire proportional chambers.

parent hyperon. Thus, each of these decay sequences has the distinctive property of having a high-momentum positive particle emerging from a negatively charged beam.

The hyperons were produced by 400-GeV/c protons incident on a Be target, 0.635 cm diameter by 15.3 cm long. The angle at which the proton beam struck the production target in the vertical plane could be set to any value from -10 to $+10$ mrad by varying currents in beam transport magnets. For this experiment data were taken at ± 5.0 and ± 7.5 mrad. The beam position and intensity at the production target were monitored by a set of ion chambers positioned just upstream of the production target.

A secondary charged beam was formed and momentum was selected by a magnetic channel M_2, which was operated at a field integral of -6.60 ± 0.01 T m, i.e., a vertically downward field, for most of the data collected. The production target, the 4-mm-diameter limiting aperture of the channel, and the exit aperture of the channel defined a circular arc through the magnet with a bend of 10 mrad for the central ray. This orbit corresponded to a momentum of 198 GeV/c. Details of the channel acceptance as a function of momentum are presented in Ref. 7.

About 20% of the data were taken at a field integral of -5.13 ± 0.01 T m, corresponding to a central momentum of 154 GeV/c (Table I).

The beam channel was followed by a 12-m-long decay volume of which 8.5 m were in vacuum, and a conventional spectrometer consisting of a magnet M_3 and eight multiwire proportional chambers (MWPC's) (C_1–C_8). M_3 was operated at a field corresponding to a transverse bending power of 0.95 GeV/c. Prompt signals were available from the MWPC's for use in the trigger electronics. In particular, C_7 and C_8 (downstream of the spectrometer magnet) had separate signals from the left and right halves to distinguish particles of negative (subscript N) and positive (subscript P) electrical charge, respectively.

Several scintillation counters (S_1–S_3) were used in the detector. S_1 signaled a particle emerging from the beam channel into the decay volume. S_2 contained a hole large enough to pass beam particles, and served to veto halo particles. S_3 was placed downstream of C_8 in the acceptance window for high-momentum particles of either sign. It was struck by beam particles, e.g., π^-,which did not decay, and the high-momentum decay products, e.g., protons, π^- and K^-.

The trigger consisted of the following combination of signals from MWPC's and scintillators:

$$T = S_1 \cdot \bar{S}_2 \cdot S_3 \cdot C_{7N} \cdot C_{7P} \cdot C_{8P} \ .$$

This trigger selected events with at least one positive and one negative particle. For some runs, the veto counter S_2 was not used. The geometry of S_3 favored events where the positive particle had reasonably high momentum. This signature was appropriate for both Ξ^- and Ω^- hyperons. As detailed in Sec. III A, approximately 9% of these triggers reconstructed as three-track events. This relatively loose trigger was chosen to minimize the possibility of trigger-induced biases in the asymmetry measurements. The trigger rate, and resulting dead time, was not a major factor in the data collection rate which was limited by the charged-particle flux, mainly π^-, through the upstream MWPC's. An auxiliary trigger,

$$\pi^- = S_1 \cdot \bar{S}_2 \cdot S_3 \ ,$$

designed to detect particles in the negative beam, was divided by a factor of 512 (or 1024 for some runs) and mixed in with the main event trigger for normalization.

TABLE I. Summary of data tapes.

Data Set	Trigger	$\int \mathbf{B} \cdot d\mathbf{l}$ (T m)	Number of data tapes at production angle (mrad) +5.0	−5.0	+7.5	−7.5
1	$S_1 \cdot S_3 \cdot C_{7N} \cdot C_{7P} \cdot C_{8P}$	−6.60	15	16		
2	$S_1 \cdot \bar{S}_2 \cdot S_3 \cdot C_{7N} \cdot C_{7P} \cdot C_{8P}$	−6.60	19	21		
3	$S_1 \cdot \bar{S}_2 \cdot S_3 \cdot C_{7N} \cdot C_{7P} \cdot C_{8P}$	−5.13	6	6		
4	$S_1 \cdot \bar{S}_2 \cdot S_3 \cdot C_{7N} \cdot C_{7P} \cdot C_{8P}$	−5.13			4	4

The data-acquisition system was CAMAC based and interfaced to a PDP-11/45 computer which recorded data on magnetic tape. The online programs monitored the performance of the detector, but did no event reconstruction. In a typical run, this system collected events at the rate of about 200 triggers per 1-sec beam spill with 2×10^8 protons on target, and required about 1.5 h to write a magnetic tape of about 75 000 events. A total of approximately 6 250 000 triggers were recorded on 91 data tapes (Table I).

III. EVENT RECONSTRUCTION AND IDENTIFICATION

The reconstruction program was designed to search for events with the topological patterns of the decay processes in Eqs. (2.1) and (2.2), i.e., two negatively charged tracks, one positively charged track and two vertices. The coordinate system used in the reconstruction had the z axis along the charged-beam direction as it emerged from the magnetic channel. The y axis was vertically upward, and the x axis was horizontal, completing a right-handed system.

A. Processing of raw event data

Wire hits from the MWPC's were converted to x-y positions in each of the chamber planes. The first-level data filtering was based on the hit patterns in C_3-C_8. Approximately 62% of the triggers lacked the hit topology essential for three tracks and were rejected at this level. The next step was to search for three tracks in the vertical, nonbend view (y-z plane), based on best fits to straight lines. About 22% more of the triggers failed at this stage. In the third step, upstream track segments in C_3-C_5 were linked to downstream track segments in C_4-C_8 at the bend plane of M_3. Roughly 7% failed the matching criteria required at this stage. The remaining $\sim9\%$ of the events constitute the three-track sample.

For each three-track event, a tentative Λ vertex was chosen as the closest approach of the positive track to the lower-momentum negative track, and the Ω^- (or Ξ^-) vertex as the closest approach of the reconstructed Λ trajectory to the remaining negative track. If the Λ vertex was found to be upstream of the Ω^- vertex, the negative tracks were interchanged and the vertices recalculated. This effect is seen in the Ξ^-, where greater statistics permit more detailed studies, and in the Monte Carlo events. It depends on momentum in two ways which tend to cancel, viz., higher momenta have smaller opening angles which enhance the effect, but also have greater distances between vertices which diminishes the effect. On a long-distance scale, this is very similar to the well-known situation encountered in searching for secondary vertices due to the decay of heavy-quark states. The probability of confusion is roughly the transverse spatial resolution, 1–2 mm, divided by $c\tau=79$ mm for the Λ. Only events with the Λ vertex downstream of the Ω^- vertex were retained.

A geometric χ^2, based on the track parameters, chamber hits, and vertices was computed, typically based on 28 degrees of freedom. Roughly 9% of the three-track events had $\chi^2>100$ and were eliminated at this stage. The geometric χ^2 distribution of the remaining events is shown in Fig. 2.

For the remaining events, the field strength of M_3 and the slopes of the tracks were used to compute the three-momenta of the tracks. The momentum vectors, in turn, were used to compute the invariant mass of the candidate Λ under the hypothesis that the positive and negative tracks were a proton and a π^-, respectively. The resulting invariant-mass distribution is shown in Fig. 3. The events were also subjected to a kinematic χ^2 fit, with the Λ mass as a constraint. This kinematic χ^2 distribution is shown in Fig. 4.

The 377 337 three-track events which passed all the above criteria were recorded on data summary tapes. The results of the first-level analysis (geometric χ^2, vertex positions, the charged-particle momentum vectors, the reconstructed Λ mass, the fitted Λ momentum vector, and kinematic χ^2) were passed on to the later analysis procedure.

B. External Monte Carlo simulation

The performance of the reconstruction programs was studied with a sample of events generated by a Monte Carlo program which simulated the experiment as closely as possible. In order to distinguish this from a hybrid Monte Carlo procedure built into the polarization analysis programs, we will refer to this as the external Monte Carlo simulation. The program generated events with distributions and cuts appropriate to (1) the observed proton beam-spot size at the production target and the length of the target, (2) passage of the parent particle (Ω^-) through the beam-channel apertures, (3) exponential decay with proper time from production of the

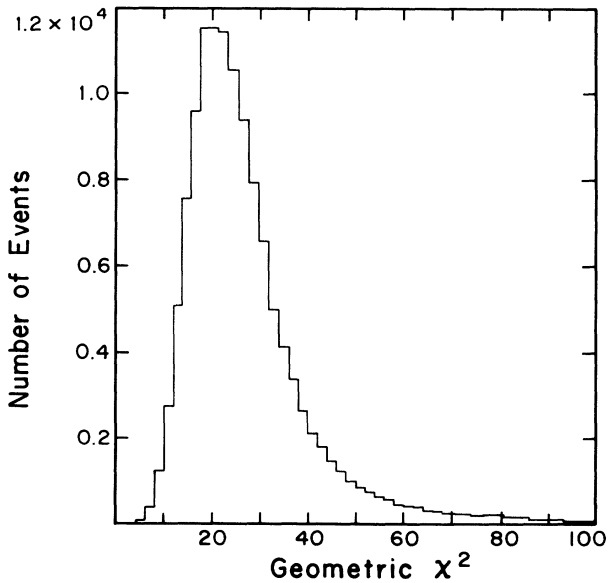

FIG. 2. The geometric χ^2 distribution for three-track events with positive vertex separation. Typically, there were 28 degrees of freedom for these events.

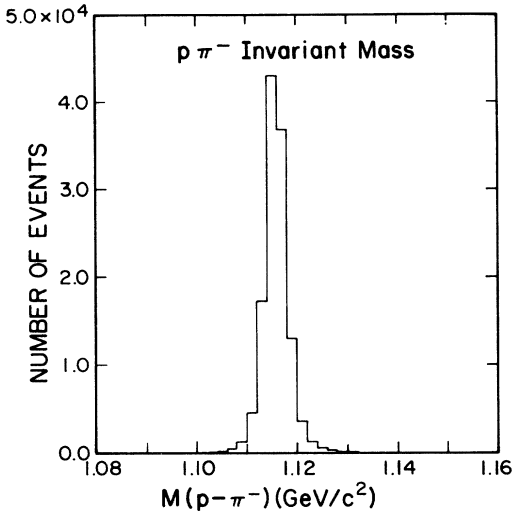

FIG. 3. The p-π^- invariant-mass distribution for events with geometric $\chi^2 < 100$ and positive vertex separation.

observed $\Omega^- \to \Lambda K^-$ events, including decays within the beam channel, (4) subsequent decays of daughter particles, $\Lambda \to p\pi^-$, (5) passage of all decay products through appropriate apertures in the apparatus, including the beam channel, trigger counters and MWPC's, and the spectrometer magnet, (6) measured inefficiencies, double-wire hit distributions of the MWPC's, and random noise hits unconnected with the event, (7) multiple Coulomb scattering for charged particles, (8) measured spatial field inhomogeneities and random fluctuations of the field with time (up to 0.5%) for the spectrometer magnet, M_3, (9) polarizations and decay asymmetries of the parent Ω^- and daughter Λ, and (10) experimental trigger requirements. The responses of the simulated detector for events generated according to these criteria were recorded on tape for analysis by the standard reconstruction programs. The generated quantities, such as positions, momenta, and decay angles, of each event were also recorded for comparison with the results of the reconstruction programs. The characteristics of the Monte Carlo events matched those of the data quite well in all measurable quantities studied such as spatial distributions, number of wires per hit, hits found per track, χ^2 for the geometric fits, and so on.

The reconstruction efficiency was determined to be 77% for the Monte Carlo events. 8% failed because of too-many or too-few wire hits. Another 10% failed because of the small opening angle(s) between two or more tracks, which resulted in misidentification of upstream and downstream track segments at the band vertex. The remaining 5% of losses were three-track events with wire hits assigned to the wrong track, which usually gave a geometric $\chi^2 > 100$.

The same Monte Carlo procedures were used to study various sources of background: $\Xi^- \to \Lambda\pi^-$, $K^- \to \pi^+\pi^-\pi^-$, $\Omega^- \to \Xi^-\pi^0$, and $\Omega^- \to \Xi^0\pi^-$.

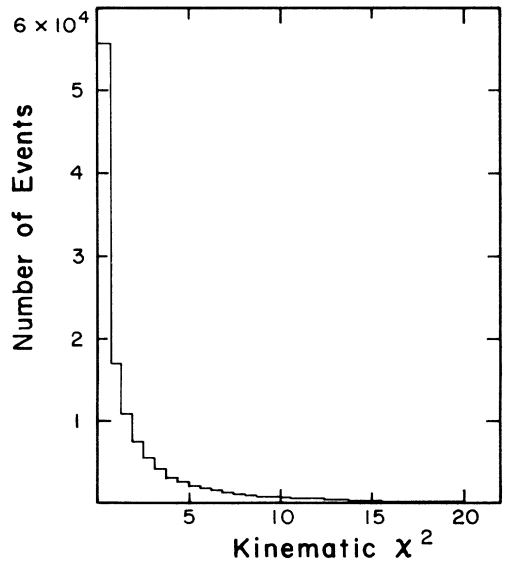

FIG. 4. The kinematic χ^2 distribution for p-π^- constrained to fit the Λ mass. This fit has one degree of freedom.

C. Reconstruction and identification of Ω^-

Events on the data summary tapes were subjected to kinematic reconstruction under each of the two hypotheses $\Omega^- \to \Lambda K^-$ and $\Xi^- \to \Lambda\pi^-$, using the fitted Λ momentum vectors. In addition, the decay angles in the rest frame of the reconstructed parent Ω^- were computed. These calculations completed the set of quantities used to reduce backgrounds, identify Ω^-, and extract the various physics results. At this point, the numbers of the three dominant event populations were approximately 374 000 $\Xi^- \to \Lambda\pi^-$, 3000 $\Omega^- > \Lambda K^-$, and 300 $\Omega^- \to \Xi^0\pi^-$. We estimate the sum of contributions from other decays with the correct topology to be less than 300. The cuts used to extract a clean sample of $\Omega^- \to \Lambda K^-$ are summarized in Table II and are discussed in detail in the paragraphs below.

1. Mass cut to select Λ

The $p\pi^-$ invariant mass for each event was required to be within ± 7.5 MeV/c^2 ($\sim 3\sigma$) of the Λ mass. Although this cut was strongly correlated with the kinematic χ^2 cut previously applied in the analysis of raw data tapes, some remaining events with large reconstruction uncertainties were cut by the mass requirement. Figure 5 shows the ΛK^- invariant-mass spectrum after this cut. There is a significant Ω^- signal on top of a large background.

2. Mass cut to eliminate Ξ^-

The $\Lambda\pi^-$ invariant mass was required to be greater than 1.345 GeV/c^2. This cut eliminated most of the $\Xi^- \to \Lambda\pi^-$ which dominated the sample. The mass spectrum for this hypothesis and the cut position are shown in Fig. 6. Figure 7 shows the ΛK^- invariant-mass spectrum for the events remaining after this cut. The Ω^- signal is now dominant, but there is still a significant background.

TABLE II. Effect of cuts on full data sample and Monte Carlo Ω^- and Ξ^-.

Cut	Real events left	Fraction of Monte Carlo events left			
		$\Xi^-\to\Lambda\pi^-$	$\Omega^-\to\Xi^0\pi^-$	$\Omega^-\to\Lambda K^-$	Other
Before cuts	377 337	1.00	1.00	1.00	1.00
(1) $1.108<M(p\pi)<1.123$ GeV	340 153	0.925	0.924	0.922	
(2) $M(\Lambda\pi)>1.345$ GeV	16 940	0.020	0.920	0.794	~ 0
(3) Decay vertex $Z>0$	6 390	0.016	0.679	0.634	
(4) $\cos\theta_\Lambda<0.4$	3 961	0.008	0.374	0.628	
(5) Production target	2 812	0.004	0.348	0.616	
(6) Decay angles	2 340	0.001	0.342	0.602	
(7) Final mass cut	1 743	0.000 07	0.111	0.556	
Estimated number of events					
Before cuts		374 000	300	3 000	300
After cuts		26	32	1 685	0

3. *Decay vertex cut*

The Ω^- decay vertex was required to be downstream of the exit aperture of the beam channel in order to ensure that all particles in the sample passed through the full length of the magnetic field.

4. *Angular cut in the Ξ^- rest frame*

Monte Carlo studies indicated that the above cuts reduced to negligible amounts the backgrounds from $K^-\to\pi^+\pi^-\pi^-$ and $\Omega^-\to\Xi^-\pi^0$ decays, but that 68% of the background from $\Omega^-\to\Xi^0\pi^-$ remained. It was established that, in the rest frame computed under the $\Xi^-\to\Lambda\pi^-$ hypothesis, the $\Omega^-\to\Lambda K^-$ events were restricted to the region $-1<\cos\theta_\Lambda<-0.4$, where θ_Λ is the angle between the c.m. Λ momentum and the laboratory z axis. Although their distribution peaked at $\cos\theta_\Lambda=-1$, the $\Omega^-\to\Xi^0\pi^-$ events covered the full range in $\cos\theta_\Lambda$, and 37% survived the cut requiring $\cos\theta_\Lambda<-0.4$.

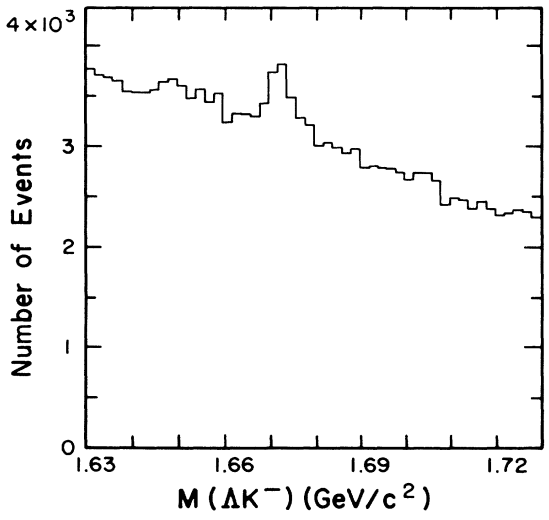

FIG. 5. The ΛK^- invariant-mass spectrum for events which passed the first of the cuts described in the text.

5. *Target-pointing cut*

The reconstructed momentum of the Ω^- was projected back through the magnetic field of the beam channel to its entrance where the production target was located. The projected position was required to be within 1 cm of the target center. This slightly reduced the $\Omega^-\to\Xi^0\pi^-$ background to about 36% of its original level, and also reduced collimator-produced events. (Figure 3.18 of Ref. 6 shows the target-pointing distribution.)

6. *Cuts on Ω^- c.m. decay angles*

Under the hypothesis $\Omega^-\to\Lambda K^-$ the c.m. decay angles θ_K and ϕ_K were computed, where θ_K is the angle between the K^- momentum and the z axis, and ϕ_K is the azimuthal angle of the K^- momentum in the x-y plane.

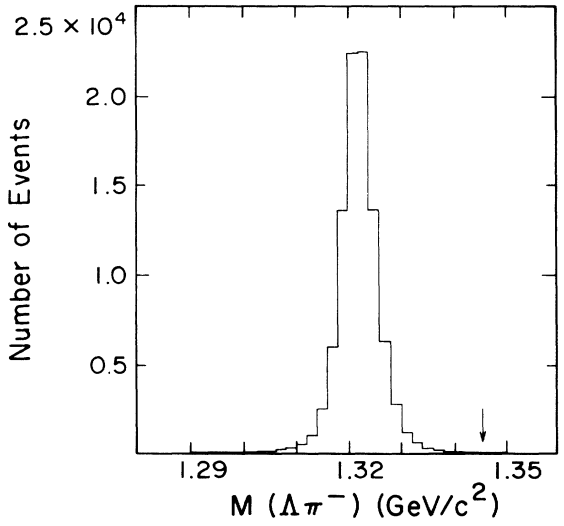

FIG. 6. The $\Lambda\pi^-$ invariant-mass spectrum for events which passed the first of the cuts described in the text, i.e., a mass cut to select daughter Λ's. Subsequently, events below the arrow were cut to eliminate Ξ^- from the sample.

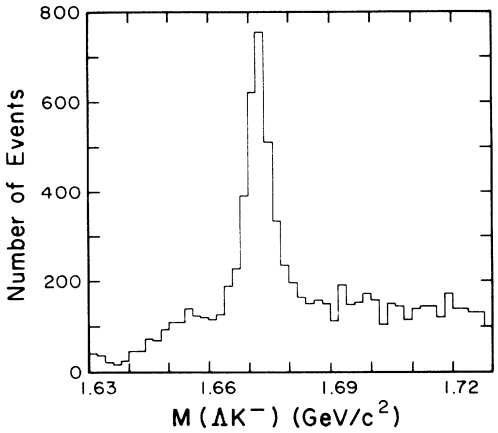

FIG. 7. The ΛK^- invariant-mass spectrum for events which passed the second of the cuts described in the text, i.e., a mass cut to eliminate Ξ^-'s.

Here, the c.m. coordinate axes are parallel to the lab axes. A scatter plot of the two-dimensional distribution of events remaining at this stage is shown in Fig. 8. Monte Carlo studies showed that the events clustered in the vicinity of $\phi_K = 0$, $\cos\theta_K = -1$ were $\Xi^- \to \Lambda\pi^-$ decays in the collimator channel. These events were eliminated by a cut along the contour shown in Fig. 8

7. *Final cut on Ω^- mass*

The ΛK^- invariant-mass distribution for events remaining after the cut above is shown in Fig. 9. Note that a semilogarithmic plot is needed to provide a significant display of the small remaining background.

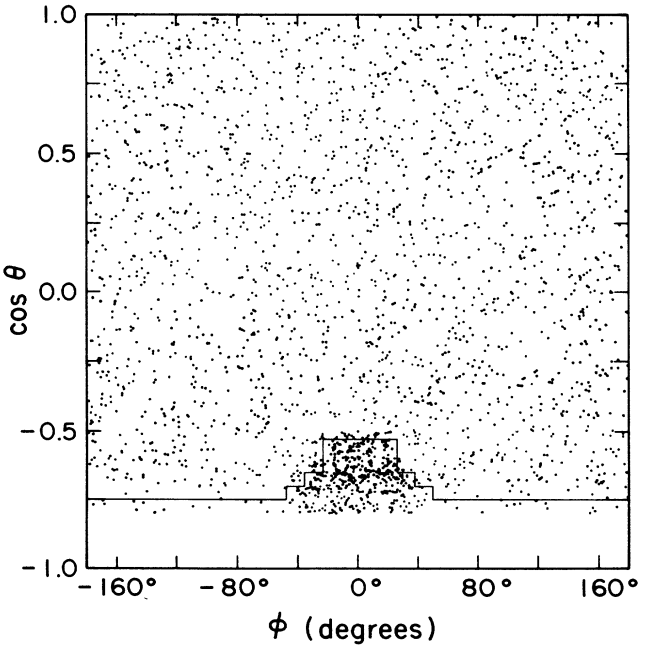

FIG. 8. A scatter plot of the angular distribution of the K^- in the Ω^- rest frame for events which satisfied cuts up to the fourth described in the text.

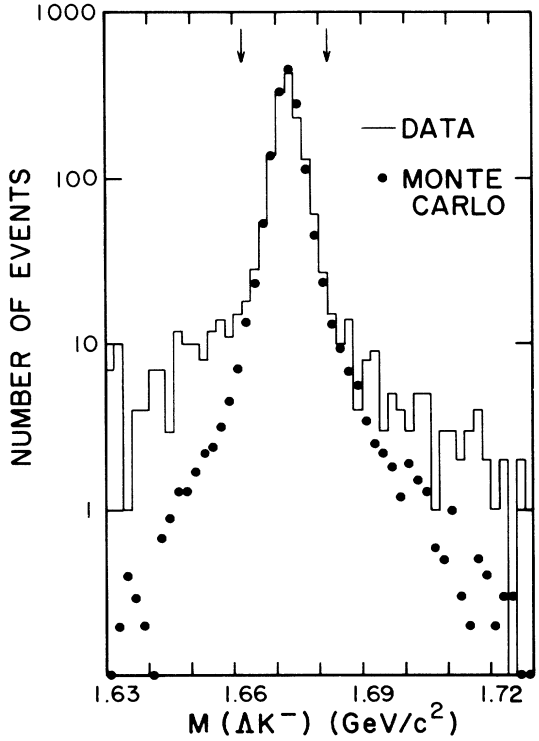

FIG. 9. The ΛK^- invariant-mass spectrum for events which passed all cuts described in the text except the final mass cut. The arrows indicate the position of the mass cut. In this final mass plot, the vertical scale is logarithmic in order to give a clearer picture of the remaining background.

The mass distribution has a full width at half maximum (FWHM) of 5.8 MeV/c^2. Cuts were made at ± 10 MeV/c^2 about the Ω^- mass (1.6725 GeV/c^2), leaving 1743 events. The distribution of these events among the various running conditions is shown in Table III.

D. Backgrounds and efficiency

In order to estimate background, an analytic curve consisting of a linear part, a Gaussian and a Lorentzian with the same width was fitted to the experimental mass distribution (Fig. 9) from 1.63 to 1.73 GeV/c^2. The background was estimated from the linear part of the fit to be 58 ± 8 events, or 3.3% of the sample. Based on Monte Carlo studies, roughly half this is due to $\Omega^- \to \Xi^0\pi^-$. The remainder are most likely poorly reconstructed $\Xi^- \to \Lambda\pi^-$ events.

Monte Carlo studies indicate that 44.4% of the $\Omega^- \to \Lambda K^-$ events were lost by the cuts described in this

TABLE III. Number of events in final sample under various running conditions.

	Production angle (mrad)			
$\int \mathbf{B}\cdot d\mathbf{l}$ (T m)	5.0	−5.0	7.5	−7.5
−6.60	667	651		
−5.13	122	128	81	94

section. Table II gives a summary of the event status and the good event and background losses at each stage of the cuts.

E. Comparison between Monte Carlo and real events

The final sample of events was compared with the external Monte Carlo events in a number of distributions. These included geometric and kinematic χ^2 distributions, proton, pion, and kaon momentum distributions, $p\pi^-$ and ΛK^- mass distributions, and the Ω^- momentum distribution. Agreement was excellent in all cases. Figure 9 is an example. (The other distributions can be found in Figs. 3.13–3.20 of Ref. 7.)

IV. LIFETIME

In principle, the lifetime of an unstable particle in flight can be measured by using the exponential decay law

$$N(z)=N(0)e^{-(mz/p\tau)} , \tag{4.1}$$

where $N(z)$ is the number of particles which survive to a distance z from a given reference point, $z=0$, and m, p, and τ are the mass, momentum, and lifetime of the particle. In practice, beams of particles are produced with a range of momenta and detected by devices with imperfect acceptance. Equation (4.1) must be modified to represent the observed distribution

$$N_R(p,z)=\epsilon(p,z)N_R(p,0)e^{-(mz/p\tau)} , \tag{4.2}$$

where $\epsilon(p,z)$ is the apparatus acceptance. For this analysis, the reference point was $z=0$ m, i.e., a point at the exit of the beam channel, M_2.

The product $\epsilon(p,z)N_R(p,0)$ was determined by a Monte Carlo (MC) calculation in which events were generated with approximately the correct momentum spectrum at the production target and with a generating Ω^- lifetime τ_0 yielding

$$N_{\rm MC}(\tau_0,p,z)=\epsilon(p,z)N_{\rm MC}(p,0)e^{-(mz/p\tau_0)} . \tag{4.3}$$

We assume that the MC program correctly represented the detector acceptance in Eq. (4.3). Further, we assume that, when the real and MC data are binned, the two momentum spectra are related by

$$N_{\rm MC}(p_j,0)=C_jN_R(p_j,0) , \tag{4.4}$$

where C_j are parameters (one for each momentum bin j) to be determined by the fit. The C_j reconcile both the slight difference in the shape of the momentum spectra and the much larger size (typically 15 times) of the MC samples.

The other parameter varied was $c\tau$, where c is the velocity of light. Various MC sets were generated with values of $c\tau_0$ between 2.25 and 3.50 cm. The Λ lifetime used was $c\tau_\Lambda=7.89$ (Refs. 9 and 10). We collect real and MC events into 5-GeV momentum bins and 0.5-m decay vertex position bins with the following notation: $r_{jk}=N_R(p_j,z_k)$ and $m_{jk}=N_{\rm MC}(p_j,z_k)$ summed in each bin.

The population of individual bins is low, and a least-squares minimization of χ^2, which assumes Gaussian distribution of errors, is not appropriate. Instead, we use a maximum-likelihood calculation with a Poisson error distribution.[11] The MC distribution can be used to form an estimate λ_{jk} of the expected population of a given bin by

$$\lambda_{jk}=m_{jk}C_j\frac{e^{-(z_km/p_j\tau)}}{e^{-(z_km/p_j\tau_0)}} , \tag{4.5}$$

where C_j and τ are parameters to be determined in a fit. In a given bin, the observed number of events, r_{jk}, occurs with a probability given by

$$P_{jk}=P_{r_{jk}}(\lambda_{jk})=\frac{-(\lambda_{ij})^{r_{jk}}}{r_{jk}!}e^{-\lambda_{jk}} . \tag{4.6}$$

The likelihood function can now be formed by taking the product over all bins of these Poisson probabilities, which are, through λ_{jk}, functions of C_j and τ:

$$L'(C_j,\tau)=\prod_{jk}(P_{jk}) ,$$

or, more conveniently,

$$\begin{aligned}L(C_j,\tau)&=-2\ln(L')=\sum_{jk}[\ln(P_{jk})]\\&=-2\left[\sum_{jk}r_{jk}\ln(\lambda_{jk})-\sum_{jk}\lambda_{jk}\right]+\text{const} .\end{aligned} \tag{4.7}$$

Minimizing this function is equivalent to maximizing the likelihood function. Had we started with Gaussian instead of Poisson probabilities, $L(C_j,\tau)$ (except for an additive constant) would be χ^2; and we assume that a one-standard-deviation change in a fitted parameter will raise its value by one unit, as is the case with χ^2. This has been confirmed by comparison with an actual χ^2 calculation.

Three independent MC sets with $c\tau_0=3.50$ cm, a fourth with $c\tau_0=2.25$ cm, and a fifth with $c\tau_0=2.35$ cm yielded $c\tau$ within a fraction of a standard deviation of each other. We conclude that the procedure is insensitive to the choice of $c\tau_0$. In all these MC sets, a realistic momentum spectrum was used, yielding very little variation in the fitted values of C_j over the entire momentum range. A sixth MC sample was generated with $c\tau_0=2.35$ cm, but with a drastically altered momentum spectrum. In this case, the C_j varied by a factor of 15 (0.3 at 130 GeV to 0.02 at 260 GeV), and the fitted lifetime was one standard deviation higher than our final answer. We believe this to be a systematic shift arising from the obvious invalidity (in this case) of our assumption that the C_j are constant across the 5-GeV bin width. The corresponding shift for the fit used for our final result is estimated less than 0.2 standard deviation. The studies of the stability of the answer with variation of cuts in momentum and z position was done with the MC set which had $c\tau_0=2.25$ cm. (See Table IV.) For this reason, our final answer was done with the same set. However, spot checks on cut variation were done with other MC sets to ensure that the conclusions were insensitive to the choice of the MC set.

The results of the analysis are presented in Table IV

TABLE IV. Lifetime fits for various conditions.

Mass interval (GeV/c^2)	Momentum interval (GeV/c)	Decay vertex position[c]	N_Ω^a	N_{MC}^b	$c\tau$ (cm)
1.630–1.710	130–260	1.0 m–3.4Z_D	1 209	17 796	2.465±0.108
1.662–1.682	100–290	1.0 m–3.4Z_D	1 141	17 539	2.398±0.106
1.662–1.682	130–180	1.0 m–3.4Z_D	446	6 445	2.425±0.165
1.662–1.682	180–200	1.0 m–3.4Z_D	302	4 844	2.434±0.213
1.662–1.682	197–300	1.0 m–3.4Z_D	348	5 620	2.441±0.209
1.662–1.682	130–260	0.0 m–3.4Z_D	1 630	26 992	2.564±0.090
1.662–1.682	130–260	0.5 m–3.4Z_D	1 354	21 620	2.505±0.099
1.662–1.682	130–260	0.75 m–3.4Z_D	1 214	19 167	2.494±0.106
1.662–1.682	130–260	2.0 m–3.4Z_D	724	10 952	2.445±0.152
1.662–1.682	130–260	1.0 m–3.0Z_D	1 075	16 680	2.410±0.120
1.662–1.682	130–260	1.0 m–4.0Z_D	1 109	17 092	2.385±0.097
1.662–1.682	130–260	1.0 m–3.4Z_D	1 096	16 909	2.432±0.112[d]

[a]Number of events satisfying cuts.
[b]Number of Monte Carlo events satisfying cuts.
[c]Downstream boundary was the smaller of 12.0 m or the given number of decay lengths, Z_D.
[d]Fit chosen for final result.

and in Figs. 10 and 11 which show the comparison between MC and real distributions for the Ω^- and daughter-Λ decay vertices, respectively.

Errors in the magnetic field of M_3 directly affect the lifetime. The current was monitored for stability at the beginning and end of each run (data tape) throughout the experiment. It fluctuated less than 0.5% about the nominal setting. The dominant spatial nonuniformity was a sextupole component, determined by two methods which agreed: a field map and analysis of trajectories through the magnet. The largest deviation from the nominal field was about 1%, and the average less than 0.25%. Its magnitude and stability were verified by the tape-to-tape agreement between known particle masses and the mass peaks for Λ, Ω^-, and Ξ^- which are also affected by field errors. We estimate the systematic uncertainty in the lifetime due to magnetic field errors to be less than 0.5%, negligible compared to the statistical uncertainty. This

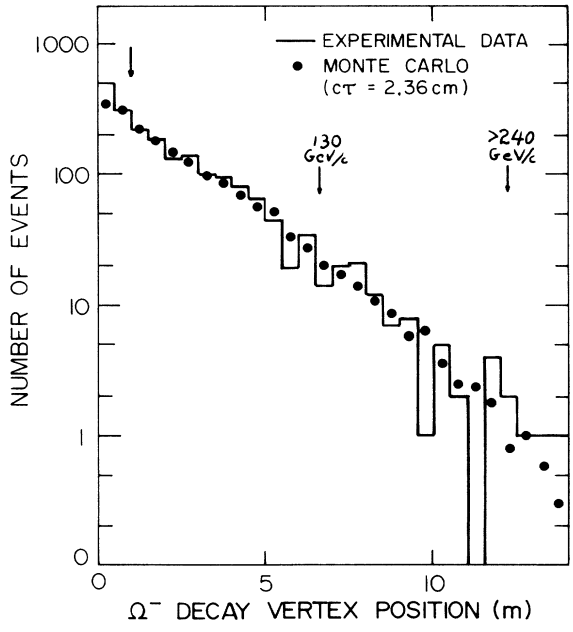

FIG. 10. The decay-vertex distribution of the Ω^- compared with the Monte Carlo calculation using $c\tau=2.36$ cm. The arrows show the region used in the fit. The downstream boundary, which varied with momentum, was the smaller of 3.4 decay lengths or 12.0 m.

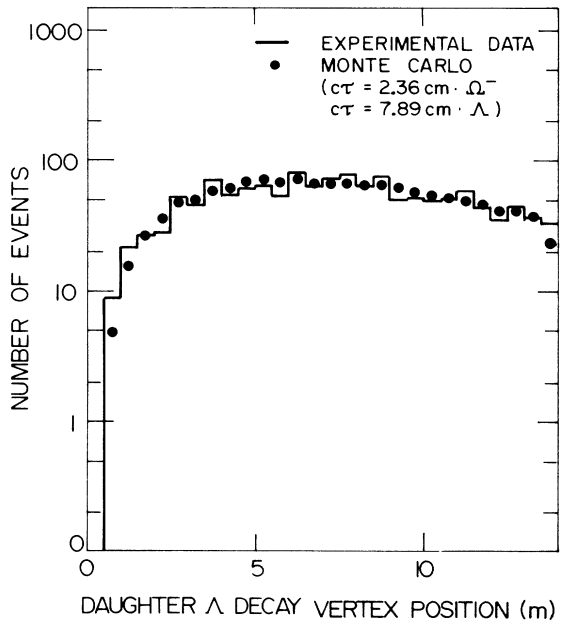

FIG. 11. The distribution of daughter-Λ decay vertices compared with the Monte Carlo calculation using $c\tau_\Omega=2.36$ cm and $c\tau_\Lambda=7.89$ cm. Only the events which fell between the arrows in Fig. 10 were used for this histogram.

was verified by Monte Carlo studies of field errors.

The stability of the answer was studied by analyzing the data with different bounds on the decay region, different bin widths, different mass cuts and different momentum intervals. A sampling of these studies is given in Table IV. The z interval from 0 to 0.5 m contained the beam-channel exit and the thickest in-beam detector, both potential background sources. The uncertainty in z was about 0.25 m. The fitted value of $c\tau$ showed a drop of about 0.1 cm as the cut on the start of the decay region was varied from 0 to 1.0 m and was stable thereafter. The final value selected was 1.0 m. Similarly, the downstream boundary on the decay region was varied from 3.0 to 12.0 m. the region of stability varied with momentum in a manner consistent with a fixed number of decay lengths, z_D (assuming $c\tau=2.467$ cm). The downstream cut chosen for the full data sample was $3.4z_D$ or 12.0 m, whichever was smaller. The lifetime was analyzed for the full data sample, and for each of three momentum bins containing roughly one-third the total number of events, with a spread of about one-half standard deviation in the results. The size of mass cut was also varied to study the effects of backgrounds and no significant effect was observed. Doubling the bin widths in both p and z produced no change. In summary, these studies showed no evidence for significant systematic errors.

Our final result for the lifetime is $c\tau=2.432\pm0.112)$ cm, or $\tau=(0.811\pm0.037)\times10^{-10}$ sec, where the uncertainty is purely statistical, and systematic uncertainties are estimated to be small.

The most accurate measurements of the Ω^- lifetime are $\tau=(0.822\pm0.028)\times10^{-10}$ sec based on 2437 events[12] and $\tau=(0.823\pm0.015)\times10^{-1}$ sec based on 9875 events.[13] Our result is consistent with $c\tau=2.467$ cm, corresponding to the weighted mean of these two experiments. The weighted average of all three measurements is $\tau=(0.821\pm0.012)\times10^{-10}$ sec.

V. POLARIZATION AND DECAY ASYMMETRY

Since, in all respects, the Ω^- fits perfectly into an s-wave SU(3) decuplet, we assume that the spin is $\frac{3}{2}$ (Ref. 14). Thus, the Ω^- can have vector polarization and alignment as well as higher-order tensor polarizations. If it is produced with a nonzero production angle by strong interactions, its polarization vector must be normal to the production plane. Independent of the value of the spin, the precession of the polarization vector in a magnetic field is described by the Bargmann-Michel-Telegdi (BMT) equations,[15] the same as for the spin-$\frac{1}{2}$ hyperons.

The weak decay $\Omega^-\to\Lambda K^-$ proceeds to the final states of orbital angular momentum $L=1,2$ through the amplitudes A_L. The asymmetry parameters in the decay process can be written as

$$\alpha=\frac{2\,\mathrm{Re}(A_1^* A_2)}{|A_1|^2+|A_2|^2},\quad \beta=\frac{2\,\mathrm{Im}(A_1^* A_2)}{|A_1|^2+|A_2|^2},$$
$$\gamma=\frac{|A_1|^2-|A_2|^2}{|A_1|^2+|A_2|^2},\quad \alpha^2+\beta^2+\gamma^2=1\ . \tag{5.1}$$

We assume that $\beta\approx0$, consistent with T invariance and no final-state interactions.

Final-state interactions (FSI's) can influence our results in three ways. First, they can change the value of α, but our task is to measure the experimental value, not unfold the contribution from FSI's. Values of $|\beta|$ as large as 0.2 leave our results unchanged. Second, FSI's can give β a value different from zero which, in turn, might distort our measurement of α. The β term produces a component of the daughter-Λ polarization which behaves as $\beta(\hat{\mathbf{\Lambda}}\times\mathbf{P}_\Omega)$, perpendicular to the α term, which is $\alpha\hat{\mathbf{\Lambda}}$. If we assume β as large as 0.2, and $P_\Omega=0.12$, then this produces a polarization component of 0.024. However, our analysis tends to average this component to zero over the full solid angle. The same is true for its contribution to the polarization measurement. Third, a large value of β can diminish the value of γ, and invalidate our assumption below that $|\gamma|\approx1$ in the polarization analysis. A value of β as large as 0.2 reduces $|\gamma|$ to 0.98, producing a negligible effect on our polarization.

In this analysis the polarization (with respect to fixed laboratory coordinates) and the helicity of the daughter Λ are used to determine the vector polarization of the Ω^- and the value of the α parameter. The relationships among the decay parameters, the Ω^- polarizations, and the various measurable distributions are discussed by Byers and Fenster,[16] Ueda and Okubo,[17] and Luk.[7] In the following sections we discuss only the expressions needed for the present analysis.

A. Daughter-Λ polarization

For $\Lambda\to p\pi^-$ decay, the angular distribution of the proton in the Λ rest system is given by

$$\frac{dn}{d\Omega_p}=\frac{1}{4\pi}(1+\alpha_\Lambda\mathbf{P}_\Lambda\cdot\hat{\mathbf{p}})\ , \tag{5.2}$$

where Ω_p and $\hat{\mathbf{p}}$ are the solid angle and the direction of the proton in the Λ rest frame and α_Λ is the Λ asymmetry parameter. Since Eq. (5.2) is independent of azimuthal angle, it can be rewritten as

$$\frac{dn}{d(\cos\theta)}=\tfrac{1}{2}(1+\alpha_\Lambda\mathbf{P}_\Lambda\cdot\hat{\mathbf{n}}\cos\theta)\ , \tag{5.3}$$

where $\hat{\mathbf{n}}$ is an arbitrarily chosen unit vector and $\cos\theta=\hat{\mathbf{n}}\cdot\hat{\mathbf{p}}$. By choosing $\hat{\mathbf{n}}=\hat{\mathbf{x}}$, $\hat{\mathbf{y}}$, and $\hat{\mathbf{z}}$ parallel to the fixed laboratory axes, the Λ polarization can be determined, and by choosing $\hat{\mathbf{n}}=\hat{\mathbf{\Lambda}}$ parallel to the Λ momentum direction in the Ω^- rest frame, the Λ helicity can be determined.

In practice, Eq. (5.2) is modified by the acceptance of the apparatus. These effects can be corrected by a hybrid Monte Carlo technique.[18] In addition, biases in the polarization due to acceptance can be canceled by periodically reversing the production angle.

B. Decay parameter analysis

The measurement of the helicity of the Λ in the Ω^- rest frame is done by letting $\hat{\mathbf{n}}=\hat{\mathbf{\Lambda}}$ in Eq. (5.3). This is best understood by a Lorentz transformation from the

Ω^- rest frame along the Λ momentum direction $\hat{\Lambda}$ into the Λ rest frame. In this system, $-\hat{\Lambda}$ is the direction of the Ω^- momentum. (See Fig. 12.) The distribution of the proton with respect to $\hat{\Lambda}$ is given by

$$\frac{dn}{d(\cos\theta)} = \tfrac{1}{2}(1+\alpha_\Lambda\alpha_\Omega\cos\theta) \ . \tag{5.4}$$

This expression results from substituting $\alpha_\Lambda = \mathbf{P}_\Lambda \cdot \hat{\Lambda}$ into Eq. (5.3). This is possible because the effects of possible Ω^- polarization (a fixed direction in the laboratory) and alignment on the daughter-Λ polarization tend to average to zero because of the symmetry of the apparatus and the random orientation (relative to $\mathbf{P}_\Omega$) of $\hat{\Lambda}$ (Ref. 7).

Data taken at ± 5 and ± 7.5 mrad were combined to form a full sample of 1743 events. The distribution in $\cos\theta$ is shown in Fig. 13 along with a Monte Carlo calculation for comparison. The result of the helicity analysis is

$$\alpha_\Lambda\alpha_\Omega = -0.022 \pm 0.051 \ . \tag{5.5}$$

This can be divided by[9] $\alpha_\Lambda = 0.642 \pm 0.013$ to yield

$$\alpha_\Omega = -0.034 \pm 0.079 \ . \tag{5.6}$$

Systematic effects were studied by dividing the data into three roughly equally populated momentum bins and repeating the analysis for each bin. The results in each bin were within one standard deviation of the above result. Also, Monte Carlo studies indicated that the bias in the helicity introduced by the apparatus acceptance, reconstruction and software cuts was less than 0.01. The effects of background were studied by widening the accepted interval of ΛK^- invariant masses. The result was unchanged within statistical uncertainty. If all the background is due to Ξ^-, the effect would be to change $\alpha_\Lambda\alpha_\Omega$ by -0.003, which is negligible. Therefore, it is estimated that systematic effects are small compared to the statistical uncertainty.

The result obtained here is completely consistent with the value reported in Ref. 13 (-0.025 ± 0.028).

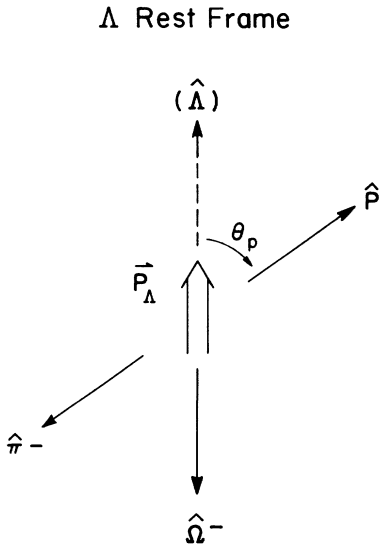

FIG. 12. Definition of unit vectors in the Λ rest frame for the determination of α_Ω. The helicity direction $\hat{\Lambda}$ is antiparallel to the Ω^- momentum vector in this system.

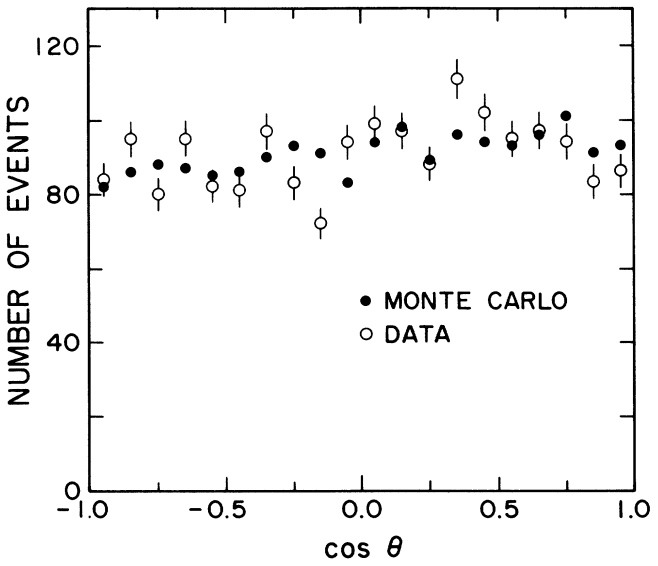

FIG. 13. The distribution of directions of daughter proton from Λ decay relative to the helicity direction defined in the text and Fig. 12. In the Monte Carlo calculation $\alpha_\Omega\alpha_\Lambda$ is assumed to be -0.022. The acceptance of the apparatus and analysis programs (including cuts) as a function of the helicity angle (not plotted and corresponding to $\alpha_\Omega\alpha_\Lambda = 0$) is nearly indistinguishable from the Monte Carlo results shown.

C. Vector polarization

Since α_Ω is small, the angular distribution of the daughter-Λ momentum vector is insensitive to the vector polarization of the Ω^-. However, the polarization of the Λ with respect to fixed laboratory axes, $\hat{\mathbf{n}} = \hat{\mathbf{x}}, \hat{\mathbf{y}}, \hat{\mathbf{z}}$, can be used to determine the Ω^- polarization. When the joint probability distribution for the decay chain is integrated over the Λ angular distribution, the angular distribution of the daughter proton is given by

$$\frac{dN}{d\Omega_p} = \frac{1}{4\pi}\left[1 + \frac{\alpha_\Lambda}{2(J+1)}[1+(2J+1)\gamma_\Omega]\mathbf{P}_\Omega \cdot \hat{\mathbf{p}}\right] . \tag{5.7}$$

A comparison between this expression and Eq. (5.2) yields the average Λ polarization

$$\mathbf{P}_\Lambda = \frac{1}{2(J+1)}[1+(2J+1)\gamma_\Omega]\mathbf{P}_\Omega \ . \tag{5.8}$$

This expression involves none of the multipole moments except the vector polarization of the Ω^-. It is a generalization of the expression used to measure the polarization of the spin-$\frac{1}{2}$ Ξ^0 hyperons,[19] and was derived in Ref. 7. From the small value of α_Ω and Eq. (5.1), we can conclude $|\gamma_\Omega| \approx 1$. Using $J = \frac{3}{2}$, Eq. (5.8) becomes

$$\mathbf{P}_\Lambda = \begin{cases} \mathbf{P}_\Omega & \text{if } \gamma_\Omega = 1 \ , \\ -0.6\mathbf{P}_\Omega & \text{if } \gamma_\Omega = -1 \ . \end{cases} \tag{5.9}$$

Thus, even though a quadratic ambiguity remains, the Λ polarization is either parallel or antiparallel to the Ω^- polarization.

If, in Eq. (5.3), we let $\hat{n}=\hat{x},\hat{y},\hat{z}$, the components of the Λ polarization along each of the three spatial axes can be determined. This was done in a manner similar to that described in Ref. 4, viz., the use of hybrid Monte Carlo techniques,[18] and bias-canceling reversals of the Ω^- production angle. The components of the Λ polarization measured in this analysis are listed in Table V. The values of $P_{\Lambda y}$ (and, thus, $P_{\Omega y}$) are consistent with zero as expected from parity conservation in the strong production process.

Parity conservation permits polarization along the x axis at the production target. Subsequent precession in the magnetic field of $M2$ can convert this to a combination of P_x and P_z in the decay region where the Ω^- are detected.

The value of α_Λ and the components of $\alpha_\Lambda P_\Lambda$ in Table V can be used to obtain the magnitudes $|P_\Lambda|=0.12\pm0.08$ at -6.60 T m, and $|P_\Lambda|=0.13\pm0.17$ at -5.13 T m.

The magnitude of the polarization is statistically consistent with zero. However, if we take the difference from zero seriously, then in both cases its direction is approximately parallel to $+\hat{x}$, and it is instructive to attempt to calculate the Ω^- production polarization and magnetic moment.

D. Precession of the polarization vector

As the Ω^-'s pass through M_2, their spin vectors in the horizontal plane precess, relative to the direction of their momentum vectors, by an amount

$$\Phi_{\text{prec}}=(q/M_\Omega c^2\beta)\left[\frac{g}{2}-1\right]\int \mathbf{B}\cdot dl$$

$$=(-0.179\ \text{rad/T m})\left[\frac{g}{2}-1\right]\int \mathbf{B}\cdot dl\ , \qquad (5.10)$$

where q and M_Ω are the charge and mass of the Ω^-, $\beta\approx1$, and g is the gyromagnetic ratio, which, for the Ω^-, is related to the magnetic moment by the equation

$$\mu_\Omega=\tfrac{1}{2}(g/2)(q/M_\Omega c)\ . \qquad (5.11)$$

If the Ω^- sample in this experiment were polarized, then Φ_{prec} is the change in the direction of polarization from production to the decay volume. The latter direction is either parallel or antiparallel to P_Λ, and the former is either parallel or antiparallel to $\hat{x}$ at the production target. (See Fig. 14.) In addition to these ambiguities, the polarization vector can precess either clockwise or anticlockwise by amounts which are known only modulo 2π rad. In principal, all the ambiguities (except the twofold ambiguity from the unknown sign of γ_Ω) can be resolved with sufficiently precise measurements at two values of $\int B\,dl$. This is illustrated for the four lowest-order ambiguities in Fig. 15.

The components P_x and P_z in Table V for each of the two values of $\int B\,dl$ were used in a least-squares fit to two parameters: the magnitude of $\alpha_\Lambda P_\Lambda$, proportional to the production polarization, and $(g/2-1)$. The data are not sufficiently precise to resolve the ambiguities. Minima in χ^2 are found at intervals of $\sim180°$ in the precession angles. The four lowest-order minima are presented in Table VI.

Figure 16 displays the contour plot of χ^2 for the two fitted variables and provides the information needed to assess the statistical significance of the data. The minima are connected by a "valley" which follows an approximately sinusoidal contour in this space. For any given value of $(g/2-1)$ the lowest point in the "valley" has a χ^2 which differs from the minimum by no more than ~3. Thus, no value of $(g/2-1)$ can be excluded at the 90% confidence level. Large values of the polarization are definitely excluded, while zero is not. This situation is well described by $\alpha_\Lambda P_\Lambda=+(0.08\pm0.05)$, or $P_\Lambda=+(0.12\pm0.07)$, where the direction is approximately $+\hat{x}$. This is the limit of what we can report purely on the basis of experimental evidence. In the following section, we attempt to draw further inferences by incorporating theoretical models.

E. Discussion

It is instructive to examine these polarization results in the light of theoretical and phenomenological expectations. Three areas of concern are discussed: the magnet-

TABLE V. Measured components of daughter-Λ polarization.

Angle (mrad)	$\int \mathbf{B}\cdot dl$ (T m)		Polarization ($\alpha_\Lambda P_\Lambda$)
5.0	-6.60	x	0.077 ± 0.055
		y	-0.002 ± 0.050
		z	-0.016 ± 0.057
5.0 and 7.5	-5.13	x	0.065 ± 0.105
		y	0.004 ± 0.102
		z	-0.054 ± 0.121

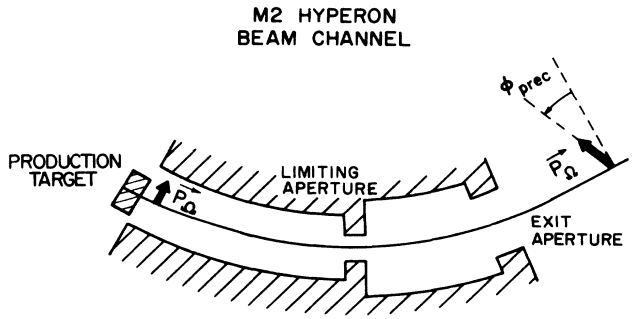

FIG. 14. The precession of the Ω^- spin polarization relative to momentum in the field of M_2. For this discussion, the coordinate system changes orientation along the Ω^- trajectory through M_2 so that $\hat{z}$ remains along the Ω^- momentum and $\hat{x}$ remains horizontal.

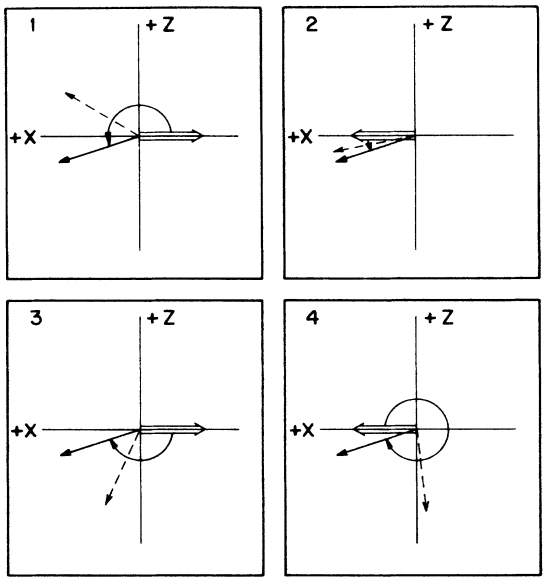

FIG. 15. The four lowest-order precession ambiguities shown for a polarization which has precessed through −6.60 T m (solid-line vector) and through −5.13 T m (dashed-line vector). The numbers labeling each diagram correspond, in order, to the solutions in Table VI.

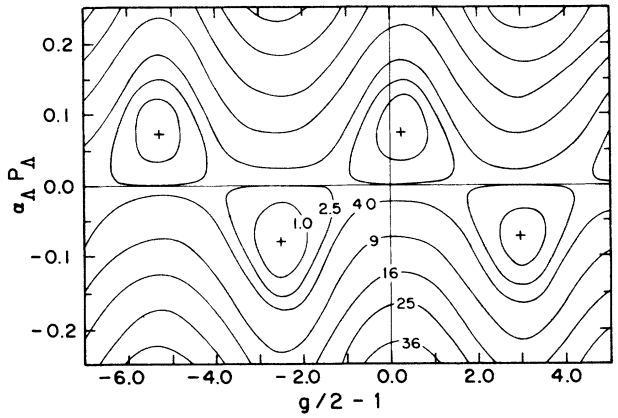

FIG. 16. Contours of χ^2 plotted as functions of $(g/2-1)$ and $\alpha_\Lambda P_\Lambda$. Each contour is labeled with the amount by which χ^2 differs from its minimum value. Thus, 1.0 corresponds to 1σ (1 standard deviation), 2.5 corresponds to $\sim 1.6\sigma$, 4.0 to 2σ, and so on.

ic moment, the Ω^- decay process, and the production polarization.

The simple broken-SU(6) quark model provides a reasonable framework for understanding baryon magnetic moments. It can account for the seven measured static moments and the Σ^0-Λ transition moment to an accuracy of about 0.2 nuclear magnetons (μ_N) (Ref. 20). For the Ω^- the theoretical prediction is

$$\mu_\Omega = 3\mu_s = 3\mu_\Lambda = -1.83\mu_N \ . \tag{5.12}$$

This favors the second solution in Table VI.

Models for Ω^- decay[21–23] predict that the processes $\Omega^- \to \Lambda K^-$, $\Omega^- \to \Xi^- \pi^0$, and $\Omega^- \to \Xi^- \pi^-$ proceed almost entirely through the parity-conserving part of the weak interactions, leading to the prediction $\alpha_\Omega \approx 0$. The result presented here and those of Ref. 13 are consistent with the prediction, but they cannot distinguish between a reaction which is parity conserving (p wave, $\gamma_\Omega = +1$), in agreement with the prediction, or parity changing (d wave, $\gamma_\Omega = -1$), in complete opposition to the prediction. However, there is no experimental evidence which contradicts the theory. Thus, in the second solution of Table VI, this theoretical consideration favors $\gamma_\Omega = +1$, and $P_\Omega = 0.12 \pm 0.08$, if the polarization is really different from zero.

A specific mechanism for this effect has been proposed by the Lund group,[24] in which the orbital and spin angular momenta of sea quarks compensate each other around the production point. This yields a spin-momentum correlation. Given the negative polarization of inclusively produced Λ (Ref. 25) the simple model accounts correctly for the signs of the other hyperon polarizations and suggests a negative polarization for inclusively produced Ω^-.

A different model for inclusive polarization has been developed by DeGrand and Miettinen.[26–28] This model includes effects of leading partons from the incident-beam particle. It has the feature that, when the projectile and produced particle share no valence quarks, the polarization of the produced particle is zero. This prediction is supported in the case of $\bar{\Lambda}$ production, which has been found to be consistent with zero.[29] It makes a definite prediction that $P_\Omega = 0$. Within 1.5 standard deviations, this is consistent with the data presented here, and it avoids the possible discrepancy which arises in the previous paragraphs.

TABLE VI. Precession fits to polarization components. For all four solutions, $\chi^2 < 0.5$. The quoted standard deviations are for an increase $\Delta\chi^2 = +1$. The uncertainties on $(g/2-1)$ are non-Gaussian and all solutions merge within 2 standard deviations ($\Delta\chi^2 = +4$). The uncertainties on the polarization are roughly Gaussian.

$g/2-1$	μ_Ω (nuclear magnetons)	P_Ω $\gamma_\Omega = +1$	P_Ω $\gamma_\Omega = -1$	Φ_{prec} (deg) −6.60 T m	Φ_{prec} (deg) −5.13 T m
2.97±0.63	−6.6±1.0	−0.11±0.08	0.18±0.13	201.1	156.3
0.25±0.58	−2.1±1.0	0.12±0.08	−0.20±0.13	16.6	12.9
−2.51±0.56	2.5±0.9	−0.12±0.08	−0.21 = −0.13	−170.1	−132.2
−5.28±0.59	7.1±1.0	0.12±0.08	−0.20±0.13	−357.6	−278.0

VI. SUMMARY

A sample of 1743 Ω^- hyperon produced by 400-GeV protons has been analyzed to yield several results. The Ω^- lifetime was measured from a subsample of 1096 events to be

$$\tau(\Omega^-)=(0.811\pm0.037)\times10^{-10}\ \text{sec}\ ,$$

in good agreement with previous measurements.[12,13]

A measurement of the helicity of the daugther Λ in the decay $\Omega^-\to\Lambda K^-$ yields the product

$$\alpha_\Lambda\alpha_\Omega=-0.022\pm0.051\ ,$$

which, using $\alpha_\Lambda=0.642\pm0.013$ (Ref. 9), yields

$$\alpha_\Omega=-0.034\pm0.079\ ,$$

also in good agreement with a previous measurement.[13]

The results of an analysis of the daughter-Λ polarization with respect to fixed laboratory coordinates are presented in Table V. The length of the Λ polarization vector is $|\mathbf{P}_\Lambda|=0.12\pm0.08$. This is not sufficiently different from zero to place a significant constraint on the Ω^- magnetic moment. If $\mu(\Omega^-)=-1.83\mu_N$ then an analysis of the precession in the magnetic field of the beam channel yields a value for the polarization of the parent Ω^- at the production target of

$$\mathbf{P}_\Omega=+0.12\pm0.08\quad(\text{if }\gamma_\Omega\approx+1)$$

or

$$\mathbf{P}_\Omega=-0.20\pm0.13\ (\text{if }\gamma_\Omega\approx-1)$$

in the parity-allowed direction. If the 1.5 standard deviations difference from zero is real, then each of the two possible values of the polarization results in some discrepancy with theory as discussed in Sec. V E. No discrepancy exists if the polarization is zero.

ACKNOWLEDGMENTS

We gratefully acknowledge the help of the staff of Fermilab, in particular the Meson Lab, during this experiment. This work was supported in part by the National Science Foundation and the Department of Energy.

---

[a]Present address: M.S. 122, Fermilab, P.O. Box 500, Batavia, IL 60510.
[b]Present address: Honeywell Corporation, MN38-1500, 10400 Yellow Circle Drive, Minnetonka, MI 55343.
[c]Present address: M.S. 222, Fermilab, P.O. Box 500, Batavia, IL 60510.
[d]Present address: Philips Medical Systems, Inc., 710 Bridgeport Avenue, Shelton, CT 06484.
[e]Present address: Physics Department, Ohio State University, Columbus, OH 43210; Mailing address: M.S. 221, Fermilab, P.O. Box 500, Batavia, IL 60510.
[f]Present address: MP-4 MS-H846, Los Alamos National Laboratory, Box 1663, Los Alamos, NM 87545.
[g]Present address: Physics Department, Rockefeller University, New York, NY 10021; Mailing address: EP Division, CERN, CH-1211, Geneva 23, Switzerland.
[h]Present address: EP Division, CERN, CH-1211, Geneva 23, Switzerland.
[i]Present address: Fonar Corporation, 110 Marcus Drive, Melville, NY 11747.

[1]C. Wilkinson *et al.*, Phys. Rev. Lett. **46**, 803 (1981).
[2]L. Deck *et al.*, Phys. Rev. D **28**, 1 (1983).
[3]R. Rameika *et al.*, Phys. Rev. Lett. **52**, 581 (1984).
[4]R. Rameika *et al.*, Phys. Rev. D **33**, 3172 (1986).
[5]Leslie L. Deck, Ph.D. thesis, Rutgers University, 1981.
[6]R. A. Rameika, Ph.D. thesis, Rutgers University, 1981.
[7]K.-B. Luk, Ph.D. thesis, Rutgers University, 1983.
[8]C. Wilkinson, Ph.D. thesis, University of Wisconsin, 1985.
[9]Particle Data Group, M. Aguilar-Benitez *et al.*, Phys. Lett. **170B**, 1 (1986).
[10]The number used is from a fit in Ref. 9. The experiments used in the fit are G. Poulard *et al.*, Phys. Lett. **46B**, 135 (1973); E. F. Clayton *et al.*, Nucl. Phys. **B95**, 130 (1975); G. Zech *et al.*, Nucl. Phys. **B194**, 413 (1977).
[11]P. R. Bevington, *Data Reduction and Error Analysis for the Physical Sciences* (McGraw-Hill, New York, 1969), pp. 110–111.
[12]M. Bourquin *et al.*, Phys. Lett. **87B**, 297 (1979).
[13]M. Bourquin *et al.*, Nucl. Phys. **B241**, 1 (1984).
[14]M. Deutschmann *et al.*, Phys. Lett. **73B**, 96 (1978); M. Baubillier *et al.*, *ibid.* **78B**, 342 (1978). Both these experiments report the Ω^- spin to be $\frac{3}{2}$ or greater.
[15]V. Bargmann, L. Michel, and V. L. Telegdi, Phys. Rev. Lett. **2**, 433 (1959).
[16]N. Byers and S. Fenster, Phys. Rev. Lett. **11**, 52 (1963).
[17]Y. Ueda and S. Okubo, Nucl. Phys. **49**, 345 (1963).
[18]G. Bunce, Nucl. Instrum. Methods **172**, 553 (1980).
[19]G. Bunce *et al.*, Phys. Lett. **86B**, 386 (1979).
[20]L. G. Pondrom, Phys. Rep. **122**, 58 (1985).
[21]M. Suzuki, Prog. Theor. Phys. **32**, 138 (1964).
[22]Y. Hara, Phys. Rev. **150**, 1175 (1966).
[23]J. Finjord, Phys. Lett. **76B**, 116 (1978).
[24]B. Andersson, G. Gustafson, and G. Ingelman, Phys. Lett. **85B**, 417 (1979); B. Andersson, G. Gustafson, and O. Mansson, Lund Report No. LU-TP-82-13, 1982 (unpublished).
[25]G. Bunce *et al.*, Phys. Rev. Lett. **36**, 1113 (1976).
[26]T. DeGrand and H. I. Miettinen, Phys. Rev. D **23**, 1227 (1981).
[27]T. DeGrand and H. I. Miettinen, Phys. Rev. D **24**, 2419 (1981); **31**, 661(E) (1985).
[28]T. DeGrand, J. Markkanen, and H. I. Miettinen, Phys. Rev. D **32**, 2445 (1985).
[29]K. Heller *et al.*, Phys. Rev. Lett. **41**, 607 (1978).